Available online at www.sciencedirect.com
ScienceDirect
Nuclear Instruments and Methods in Physics Research A 580 (2007) 925–928
NUCLEAR INSTRUMENTS & METHODS IN PHYSICS RESEARCH Section A
www.elsevier.com/locate/nima

Tomographic reconstruction of three-dimensional objects from hard X-ray differential phase contrast projection images

F. Pfeiffer*, O. Bunk, C. Kottler, C. David

Paul Scherrer Institut, CH-5232 Villigen PSI, Switzerland

Available online 12 July 2007

Abstract

We report on a method for tomographic phase contrast imaging of centimeter sized objects. As opposed to existing techniques, our approach can be used with low-brilliance, lab based X-ray sources and thus is of interest to a wide range of applications in medicine, biology, and non-destructive testing. The work is based on the recent development of a hard X-ray grating interferometer, which has been demonstrated to yield differential phase contrast projection images. Here we particularly focus on how this method can be used for tomographic reconstructions using filtered backprojection algorithms to yield quantitative volumetric information of the real part of the samples's refractive index.

PACS: 87.59.Hp; 87.59.Fm; 07.85.Fv

Keywords: X-ray tomography; Computed tomography; Phase contrast; Filtered backprojection

1. Introduction

Phase-sensitive X-ray imaging, which uses the phase shift rather than the absorption as the imaging signal, has the potential of substantially increased contrast in biological samples [1–3]. Various phase-sensitive X-ray imaging methods were developed in the past years. They can be classified into interferometric methods [4,5], techniques using an analyzer crystal [6–8], and free-space propagation methods [9–12]. Some of them have been extended to three-dimensional (3D) X-ray phase computed tomography (CT) and yield excellent results, when highly brilliant synchrotron radiation is used.

It has recently been demonstrated that laboratory based X-ray phase CT is in principle possible and can yield excellent results for microscopic samples [13,14]. However, several constraints impair the application of the existing approaches as a standard method in hospital based medical imaging. One of the most severe limitations is that the methods require sufficiently brilliant radiation, which is presently only available from sources with small enough source dimensions (typically a few microns) and correspondingly low-power (a few Watts). The limited field of view, the in-vacuum setup, and the homogeneous object [15] or pure phase object [16] approximation for the phase retrieval algorithm further restrict the existing techniques to specific micro-CT studies [14]. This is why X-ray phase tomography, despite its potential for improved contrast, is currently not available as a standard 3D characterization tool for medical, biological or industrial applications.

Here we report how an alternative approach using a hard X-ray grating interferometer can be used for quantitative CT phase reconstructions of macroscopic, centimeter sized objects with standard X-ray tube sources with square millimeter source dimensions and correspondingly high power (>1 kW). The work is based on the recent development of a hard X-ray grating interferometer, which has been demonstrated to yield two-dimensional (2D) differential phase contrast (DPC) projection images [17]. In this article we particularly focus on how the latter 2D method can be extended into 3D with an adapted filtered backprojection (FBP) reconstruction algorithm to yield

*Corresponding author.
E-mail address: franz.pfeiffer@psi.ch (F. Pfeiffer).

0168-9002/$ - see front matter © 2007 Elsevier B.V. All rights reserved.
doi:10.1016/j.nima.2007.06.104

quantitative volumetric information of the real part of the refractive index.

2. Tomographic reconstruction

Consider a 3D object described by $g(x,y,z)$ as shown in Fig. 1. The projections in a plane defined by $z=z_0$ through the object at an angle ω to the x-axis are given by the Radon transform [18]

$$\mathscr{G}(y',\omega)=\int_{-\infty}^{\infty} g(x',y')\,\mathrm{d}x' \tag{1}$$

where x' and y' denote a coordinate system which is rotated by an angle ω around the z-axis with respect to x and y. Note that we have omitted the variable z because it does not affect the further derivation. A fast and accurate algorithm for reconstructing the original object function $g(x,y)$ from the Radon transform $\mathscr{G}(y',\omega)$ is the FBP algorithm, which can be represented by the convolution backprojection integral [19,20]

$$g(x,y)=\int_0^{\pi} \mathscr{F}\mathscr{T}^{-1}[\widetilde{\mathscr{G}}(v',\omega)\cdot\widetilde{k}(v')]\,\mathrm{d}\omega \tag{2}$$

where $\widetilde{\mathscr{G}}(v',\omega)$ is the Fourier transform of $\mathscr{G}(y',\omega)$, v' the reciprocal space coordinate corresponding to $y'=-x\sin\omega+y\cos\omega$, $\widetilde{k}(v')$ is the Fourier representation of the filter function in the FBP, and $\mathscr{F}\mathscr{T}^{-1}$ is the inverse Fourier transform. For continuously sampled projection functions $\mathscr{G}(y',\omega)$, the filter is defined as $\widetilde{k}(v')\equiv|v'|$. In practise, where the projections are sampled with a finite resolution, $\Delta y'$, the filter should be truncated at the Nyquist frequency, $1/2\Delta y'$ and becomes [19]

$$\widetilde{k}(v')\equiv\begin{cases}|v'|, & |v'|\leqslant 1/2\Delta y'\\ 0, & |v'|>1/2\Delta y'\end{cases} \tag{3}$$

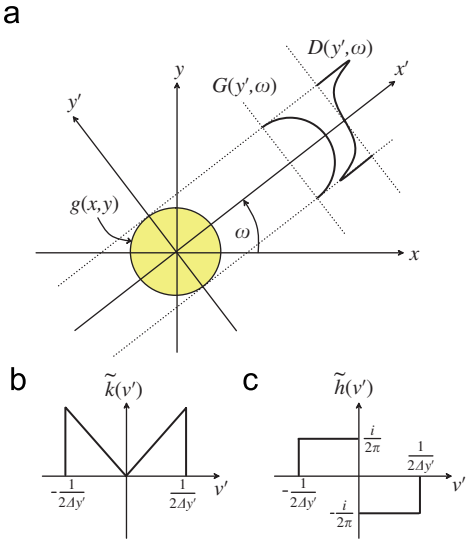

Fig. 1. Tomographic reconstruction. (a) Projection geometry. (b, c) Backprojection filter functions for (b) simple projection line integrals and (c) gradient projection integrals.

(see also Fig. 1b). Let us now consider the case, where the experimental arrangement does not only yield the ordinary line projection of the object function as defined by Eq. (1), but also the line projection of the partial derivative of the object function:

$$\mathscr{D}(y',\omega)=\int_{-\infty}^{\infty}\frac{\partial g(x',y')}{\partial y'}\,\mathrm{d}x'. \tag{4}$$

Then tomographic reconstruction based on the conventional FBP using the abovementioned linear filter function (Eq. (3)) will not result in a correct reconstruction of the original object function $g(x,y)$. In analogy to what has been suggested by Faris et al. [21] in the case of deflection tomography using visible laser light, the problem can be solved by adapting the filter function in the FBP algorithm accordingly. Using the Fourier derivative theorem we find $\widetilde{\mathscr{D}}(v',\omega)=2\pi i v'\cdot\widetilde{\mathscr{G}}(v',\omega)$, where $\widetilde{\mathscr{D}}$ is the Fourier transform of $\mathscr{D}$. Changing the integration and differentiation order in Eq. (4) and substituting into Eq. (2), we obtain

$$g(x,y)=\int_0^{\pi}\mathscr{F}\mathscr{T}^{-1}[\widetilde{\mathscr{D}}(v',\omega)\cdot\widetilde{h}(v')]\,\mathrm{d}\omega \tag{5}$$

with the DPC-FBP filter function

$$\widetilde{h}(v')\equiv\begin{cases}1/2\pi\mathrm{i}\cdot\mathrm{sgn}(v'), & |v'|\leqslant 1/2\Delta y'\\ 0, & |v'|>1/2\Delta y'\end{cases} \tag{6}$$

where $\mathrm{sgn}(v')$ is the sign function (see Fig. 1c).

3. Experimental

In practise our DPC imaging setup consists of a source grating G0, a phase grating G1, and an analyzer absorption grating G2 (Fig. 2a). The source grating (G0), typically placed close to the X-ray tube anode, is an arrayed aperture mask with transmitting slits. It effectively allows for the use of relatively large, i.e. square millimeter sized X-ray sources, without compromising on the coherence requirements of the DPC method [17,22]. The DPC itself is formed within the two gratings G1 and G2 and is similar to Schlieren imaging [23] or diffraction-enhanced imaging [6,8]. It essentially relies on the fact that a phase object placed in the X-ray beam path causes a slight deflection of the beam transmitted through the object (Fig. 2b). The fundamental idea of DPC imaging depends on locally detecting these angular deviations. The angle is directly proportional to the local gradient of the object's phase shift $\Phi(y,z)$ and can be quantified by [23]

$$\alpha(y,z)=\frac{\lambda}{2\pi}\frac{\partial\Phi(y,z)}{\partial y}=\int_{-\infty}^{\infty}\frac{\partial\delta(x,y,z)}{\partial y}\,\mathrm{d}x \tag{7}$$

where λ is the wavelength of the X-rays and $\delta(x,y,z)$ the decrement of the real part of the object's refractive index $n(x,y,z)$. As described in more detail in Ref. [24], a set of images taken for different positions of the grating G2 (phase-stepping scan) can be used to simultaneously obtain both the DPC images and the conventional transmission projections $\exp(-\int_{-\infty}^{\infty}4\pi\beta(x,y,z)/\lambda\,\mathrm{d}x)$, where $\beta(x,y,z)$

is the imaginary part of the objects refractive index distribution.

The experiments were carried out on a Seifert ID 3000 X-ray generator operated at 35 kV/30 mA. We used a tungsten (W) line focus tube (DX-W8 × 0.4-L) with a focus size of 8 (hor.) × 0.4 (ver.) mm^2. Due to the inclination of the target with respect to the optical axis of our setup of 6°, the effective source size was 0.8 (hor.) × 0.4 (ver.) mm^2. The gratings were fabricated by a process involving photolithography, deep etching into silicon and electroplating of gold. They were placed with their lines perpendicular to the optical axis of the setup and parallel to the axis of tomographic rotation [25]. The images were recorded using a 150 μm micron thick Cesium Iodide (CsI) scintillation screen with a demagnifying optical lens system and a cooled charge coupled device [26,27].

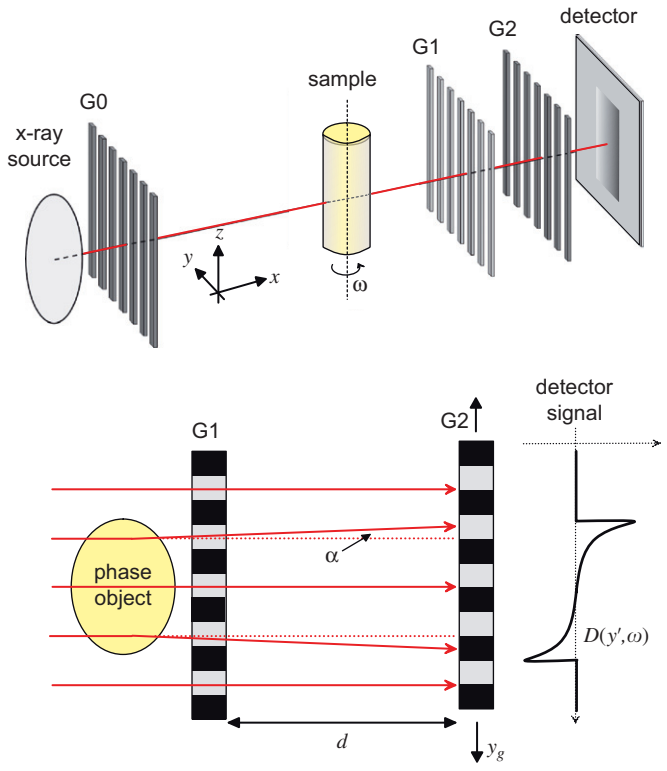

Fig. 2. X-ray imaging interferometer. (a) Setup based on three transmission gratings. (b) A phase object in the beam path causes a slight deflection of X-rays changing the locally transmitted intensity through the arrangement formed by the gratings G1 and G2.

4. Results and conclusions

Fig. 3 displays results of applying our method to a test sample—a children's confection in the form of a chocolate egg containing plastic assemblies of a small toy ('Kinder surprise egg'). It shows four (out of 360) DPC projections (Fig. 3a–d), 3D renderings of the reconstructed 3D distribution of $\delta(x, y, z)$ (Fig. 3e–g), and a photograph of the sample (Fig. 3h). The tomographic reconstruction was achieved by using the measured DPC projections as input for the DPC-FBP algorithm (Eq. (5)) with the imaginary filter function (Eq. (6)).

The results reveal details of the sample's internal structure and clearly demonstrate that a correct reconstruction of the original object was achieved. Furthermore the results show that phase contrast based CT is feasible with large objects at standard X-ray tube sources. This illustrates that our method provides an alternative approach for obtaining 3D X-ray CT information without the explicit necessity of absorbing X-rays in the object. A further development of the method towards higher X-ray energies, and correspondingly lower absorption, will potentially provide a significant dose reduction, an aspect of particular interest for medical imaging applications. This is not possible for conventional absorption based CT

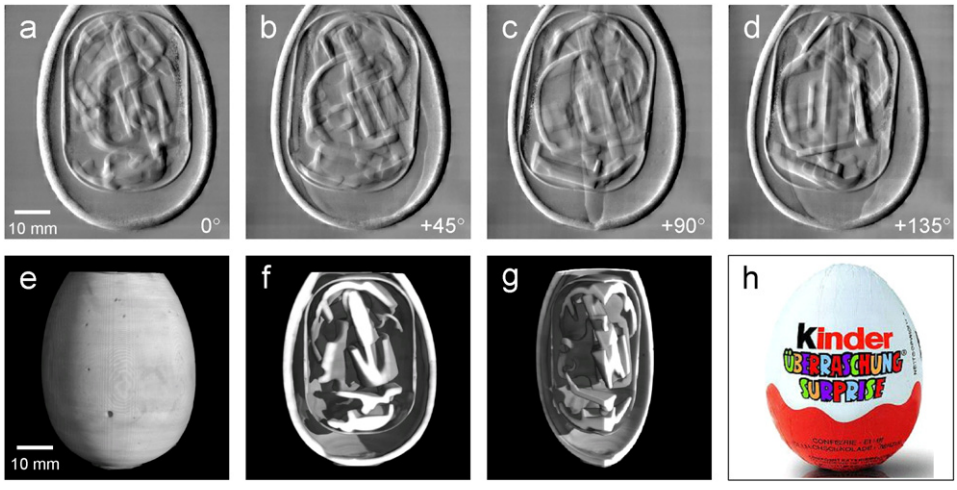

Fig. 3. Results for a test sample. (a–d) Differential phase contrast (DPC) projections recorded at different viewing angles. (e–g) Renderings of the reconstructed 3D distribution of $\delta(x, y, z)$ of the sample. (h) Photograph of the sample, a children's confection in the form of a chocolate egg containing plastic assemblies of a small toy ('Kinder surprise egg'). The volume data set of 400 × 400 × 512 voxels was reconstructed from 360 projections recorded within a total exposure time of 2 h [28].

methods, where a lower absorption in the object inevitably results in a corresponding loss of image contrast.

In conclusion we have shown how a setup consisting of three transmission gratings together with an appropriate tomographic FBP algorithm can yield 3D tomographic information based on hard X-ray DPC projections of macroscopic objects. In contrast to existing techniques [13,14] our approach can be used with conventional X-ray tube sources with square millimeter source sizes and several kW power. It is significantly more efficient, not restricted to homogeneous objects [15] or weakly absorbing objects [16], and does not require the sample to be in vacuum.

We have demonstrated the capabilities by presenting a 3D tomographic phase reconstruction of a centimeter sized test sample. Based on the results we conclude that our method represents a major step forward in X-ray phase tomography with lab based X-ray sources that provides all of the information imparted by conventional X-ray CT, with the potential of yielding additional and complementary information through the phase contrast signal. Thus, we envision a widespread application of our method in areas where X-ray phase tomography would be desirable, but is currently unavailable. For example, we believe that this method can readily be implemented without major changes to non-destructive industrial desktop tomography systems, small animal imaging, or biomedical applications. Finally, upon further development of the method for higher X-ray energies, the application in medical X-ray CT scanners can potentially yield an increased soft tissue sensitivity for X-ray CT which presently is only available through much more expensive techniques, like magneto resonance imaging (MRI).

Acknowledgements

C.K. acknowledges support through the KTI under contract No. 7796.2 DCPP-NM. We gratefully acknowledge the assistance of J. Bruder, and C. Grünzweig in the experiments and T. Weitkamp, M. Stampanoni, and P. Cloetens for fruitful discussions.

References

[1] R. Fitzgerald, Phys. Today 53 (7) (2000) 23.
[2] A. Momose, Opt. Express 11 (2003) 2303.
[3] A. Momose, Jpn. J. Appl. Phys. 44 (2005) 6355.
[4] U. Bonse, M. Hart, Appl. Phys. Lett. 6 (1965) 155.
[5] A. Momose, T. Takeda, Y. Itai, K. Hirano, Nat. Med. 2 (1996) 473.
[6] V.N. Ingal, E.A. Beliaevskaya, J. Phys. D 28 (1995) 2314.
[7] T.J. Davis, D. Gao, T.E. Gureyev, A.W. Stevenson, S.W. Wilkins, Nature 373 (1995) 595.
[8] D. Chapman, W. Thomlinson, R.E. Johnston, D. Washburn, E. Pisano, N. Gmur, Z. Zhong, R. Menk, F. Arfelli, D. Sayers, Phys. Med. Biol. 42 (1997) 2015.
[9] A. Snigirev, I. Snigireva, V. Kohn, S. Kuznetsov, I. Schelokov, Rev. Sci. Instr. 66 (1995) 5486.
[10] S.W. Wilkins, T.E. Gureyev, D. Gao, A. Pogany, A.W. Stevenson, Nature 384 (1996) 335.
[11] K.A. Nugent, T.E. Gureyev, D.F. Cookson, D. Paganin, Z. Barnea, Phys. Rev. Lett. 77 (1996) 2961.
[12] P. Cloetens, W. Ludwig, J. Baruchel, D. van Dyck, J. van Landuyt, J.P. Guigay, M. Schlenker, Appl. Phys. Lett. 75 (1999) 2912.
[13] S.C. Mayo, P.R. Miller, S.W. Wilkins, T.J. Davis, D. Gao, T.E. Gureyev, D. Pagnanin, D.J. Parry, A. Pogany, A.W. Stevenson, J. Microsc. 207 (2002) 79.
[14] S.C. Mayo, T.J. Davis, T.E. Gureyev, P.R. Miller, D. Paganin, A. Pogany, A.W. Stevenson, S.W. Wilkins, Opt. Express 11 (2003) 2289.
[15] D. Paganin, S.C. Mayo, T.E. Gureyev, P.R. Miller, S.W. Wilkins, J. Microsc. 206 (2002) 33.
[16] A.V. Bronnikov, Opt. Commun. 171 (1999) 239.
[17] F. Pfeiffer, T. Weitkamp, O. Bunk, C. David, Nat. Phys. 2 (2006) 258.
[18] J. Radon, Ber. Verh. Sächs. Akad. Wiss. Leipzig Math Nat. 69 (1917) 262.
[19] G.T. Herman, Image Reconstruction from Projections, Academic Press, New York, 1980.
[20] A.C. Kak, M. Slaney, Principles of Computerized Tomography, IEEE Press, New York, 1987.
[21] G.W. Faris, R.L. Byer, Appl. Opt. 27 (1988) 5202.
[22] F. Pfeiffer, O. Bunk, T. Weitkamp, J.F. van der Veen, I.K. Robinson, Phys. Rev. Lett. 94 (2005) 164801.
[23] M. Born, E. Wolf, Principles of Optics, Pergamon Press, Oxford, 1980.
[24] T. Weitkamp, A. Diaz, C. David, F. Pfeiffer, M. Stampanoni, P. Cloetens, E. Ziegler, Opt. Express 13 (2005) 629.
[25] They had periods of: $p_0 = 73\,\mu m$, $p_1 = 3.9\,\mu m$, and $p_2 = 2.0\,\mu m$. The height of the grating structures were 42 μm (G0), 35 μm (G1), and 26 μm (G2). The distances between the gratings were $l = 1.57\,m$ and $d = 43\,mm$.
[26] The effective spatial resolution was mainly determined by the thickness of the scintillation screen to $\approx 0.1\,mm$. The field of view is currently limited by the 100 mm wafer processing technology to $64 \times 64\,mm^2$. No principle constraints hinder the upscaling by using state-of-the-art (300 mm) techniques.
[27] Fingerlakes Instruments, FLI IMG 1001, KODAK chip with 1024×1024 pixels, $24 \times 24\,\mu m^2$ pixel size.
[28] For one projection, four individual raw images (phase-stepping) with exposure times of 5 s each were recorded. The total exposure time can be greatly reduced by (a) using a more efficient detector, (b) decreasing the distance between the source and the sample, and (c) using standard rotating anode X-ray generators with a power of several kW.